The Pennsylvania State University
College of Earth and Mineral Sciences
Department of Geosciences

A QUANTITATIVE ANALYSIS OF DEEP SHALE WEATHERING AT THE SHALE HILLS CRITICAL ZONE OBSERVATORY

A Senior Thesis in Geosciences

by

Molly E. Holleran

Submitted in Partial Fulfillment
of the Requirements
for the Degree of

Bachelor of Science

May, 2011

We approve this thesis:

_____	_____
Susan L. Brantley, Professor of Geosciences	Date
_____	_____
David M. Bice, Professor of Geosciences Associate Head of the Undergraduate Program	Date

ABSTRACT

In this study we demonstrate that the geochemical weathering of the Silurian Rose Hill Shale Formation has caused mineralogical changes with depth into bedrock at the Susquehanna Shale Hills Observatory (SSHO), a forested first-order watershed in central Pennsylvania, U.S.A.. Established as a member of the Critical Zone Exploration Network, SSHO is under investigation in attempts to tie relationships between geochemistry, hydrology, ecology and geomorphology on a watershed scale. The geochemical alteration of shale under aqueous conditions induces chemical reaction fronts with depth. Chemical reaction fronts are defined in this study as depths associated with the depletion of a particular mineral or element, in comparison to the parent bedrock.

Mineral weathering fronts were identified in drilled samples from the valley floor, based on geochemical and mineralogical characterizations. Seventeen samples from a 16 meter deep drill core taken at the valley floor site were analyzed and compared to similar samples from the ridge top. A carbonate weathering front was identified at 3 m depth, an illite weathering front at 4 m depth, and a pyrite oxidation front and ferrous-ferric transition at 7 m depth in the valley floor of SSHO. Identical reaction fronts were identified at the ridge top of the SSHO catchment, although at variable depths. Ridge top carbonate weathering front is noted at 25 m, pyrite oxidation front an ferrous-ferric transition at 25 m and illite weathering front at 0.5 m. Elemental concentration remains constant with depth, with the exception of Ca showing the highest variation. Presence of kaolinite and vermiculite is observed within the upper 4 meters in the valley floor, associated with the extent of the illite weathering front.

LIST AND DISCRIPTION OF FIGURES:

ACKNOWLEDGEMENTS

I'd like to most importantly thank my advisor and mentor who has been enthusiastically shaping me into a *confident* female geoscientist throughout the past few years, Sue Brantley. Sue has continuously encouraged me to push myself, and has prepared me for my graduate school journey in more ways than she'll know. Similarly this thesis would have not been complete if it not for the previous research from Lixin Jin. My first year or two at Penn State was spent as Lixin's constant following shadow, whether it be in the field, laboratory or office. Lixin utilized my early undergraduate inexperience and turned me into a savvy field and lab tech.

I'd also like to thank other members of the Brantley lab group for supporting me over the years, Laura Liermann, Jennifer Williams, Lin Ma, Katya Bazilevskaya, Ashlee Dere, Elizabeth Herndon, Tiffany Yesavage, Nikki West, Megan Carter-Thomas and Joe Orlando. Who have all become like a second family to me throughout the past years. Henry Gong for assisting with the ICP-AES analysis. Nichole Wonderling for assistance with XRD training and sample analysis. Kamini Singha for facilitating the well drilling within SSHO, without which I would have had no samples to base this thesis from. Additionally Kamini enthusiastically provided televiewer images and the natural gamma log from the drilled wells. Peter Heaney for assisting with my understanding of some of my acquired XRD data and George Holmes for providing depth to water table data, and supplemental SSHO maps of wells.

1. Introduction

The chemical weathering of bedrock provides insights into rates of mineral transformations and establishment of geochemical reaction fonts. On a geologic time scale, weathering rates serve as a both mechanical and chemical controls on landscape evolution and geomorphology, defining the Critical Zone (Riebe et al. 2003; Brantley et al. 2006: Anderson et al., 2007). Weathering of shale yields changes in mineralogy with depth into bedrock. Therefore geochemical alteration of shale under aqueous conditions induces chemical reaction fronts with depth. Chemical reaction fronts are defined in this study as depths associated with the depletion of a particular species, in comparison with the parent material. Determining an accurate parent material composition provides a reference for documenting mineralogical changes within a studied profile (Tuttle et al. 2009).

The Shale Hills Critical Zone Observatory (SSHO) in part was established to further investigate the strong ties between geochemistry, hydrology, ecology, and geomorphology in a forested catchment that is developed on shale. Jin et al. (2010) has summarized major mineral transformations occurring in the Rose Hill Shale in the SSHO. Specifically they report the following reactions occurring at the ridge top the of the catchment (DC1) as,

i.) feldspars → kaolinite,

ii.) illite → vermiculite,

iii.) chlorite → vermiculite

This study aims to give a quantitative analysis of deep shale weathering fronts that are representative in the valley of the catchment in comparison to observations previously reported for drilled ridge top samples. The goals of this study are to (1) identify chemical profiles as a

function of depth in the valley floor; (2) identify mineralogical and geochemical reaction fronts in the profiles; (3) synthesize data from ridge top to valley floor into an understanding of weathering in the catchment as one system.

2. Methods

2.1. Site description

The geochemical properties of shale weathering have been explored by the analysis of drilled samples collected from the valley floor of Susquehanna/ Shale Hills Critical Zone Observatory. Located within the Valley and Ridge province in central Pennsylvania, this catchment experiences a generally temperate climate with a mean annual temperature of 10^{o}C (Jin et al., 2010). Snow cover in the area is typical from December to mid March. The bedrock lithology of SSHO consists of relatively steeply dipping Silurian age shales of the Rose Hill Formation (Fold, 1960; Lynch, 1976). Bedrock has a gentle dip of 25°, consistent with bore hole televiewer data and measurements reported on geological maps (Hoskins, 1973). The elevation of the catchment ranges from 310 m at the highest point to 256 at the outlet (Lin et al., 2006). The catchment is V-shaped, characterized by a system of 1D ridges, 2-D planar hill slopes and 3-D convergent swale hill slopes (Jin et al., 2010, see Figure 1). The catchment is oriented in an east-west direction, defined by the north-facing and south-facing slopes with a small 1D, seasonally flowing stream (Lin et al., 2006).

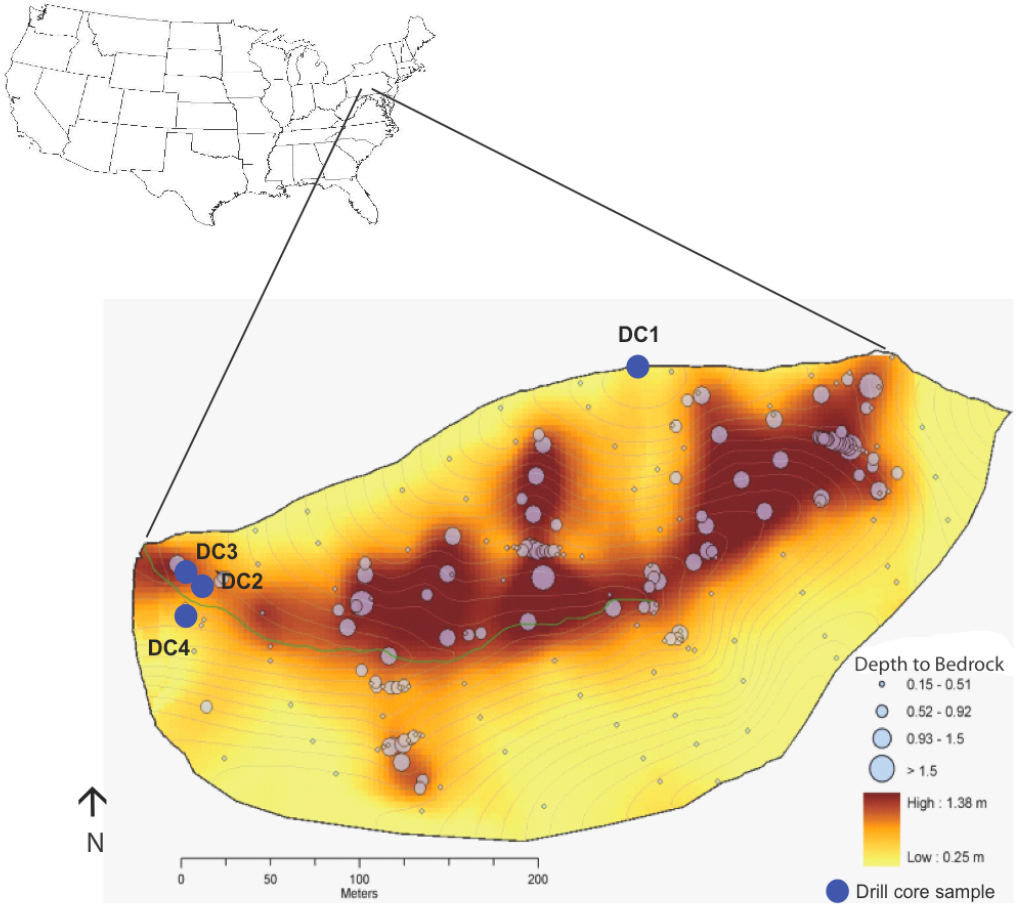

Figure 1: Map of Shale Hills Critical Zone Observatory (modified from Lin et al. 2006), SSHO is a 7.9-hectare forested watershed located in Huntingdon County, PA. Drill core samples were taken at locations indicated by blue circles, DC1 is termed the ridge top and DC3, DC2, and DC4 are valley floor sites. Background shading represents the depth to bedrock in the catchment.

2.2 Drill core

Using a direct rotary air drill, a drilling team led by K. Singha (Penn State) drilled 16 meters into the bedrock at the valley floor of the catchment in August 2008. Four wells were drilled in the valley floor; DC2, DC3, DC4, DC5 (Fig. 1). These four drilled wells are closely spaced (3>m apart); furthermore, three were drilled on the northern side of the first order stream and one on the southern side of the stream. This study reports chemical and mineralogical results focused on DC3, with additional data from Jin et al. (2010), the DC1 core located at the ridge top for comparison. Rock chips were directly sampled from the drill at quarter meter intervals; as depth into bedrock increased to 12 m, samples were taken approximately every meter. Field notes indicate the water table was encountered at 3.6-3.8 m (12-13 feet) as samples transitioned from dry to wet. All samples taken were initially assumed to be of the Rose Hill Formation, although the interface between Rose Hill and the underlying Keefer Formation has been thought to be at the deepest most drill core samples (15m). Height of the well casing was corrected for samples taken in the field for the correct depth of sampling.

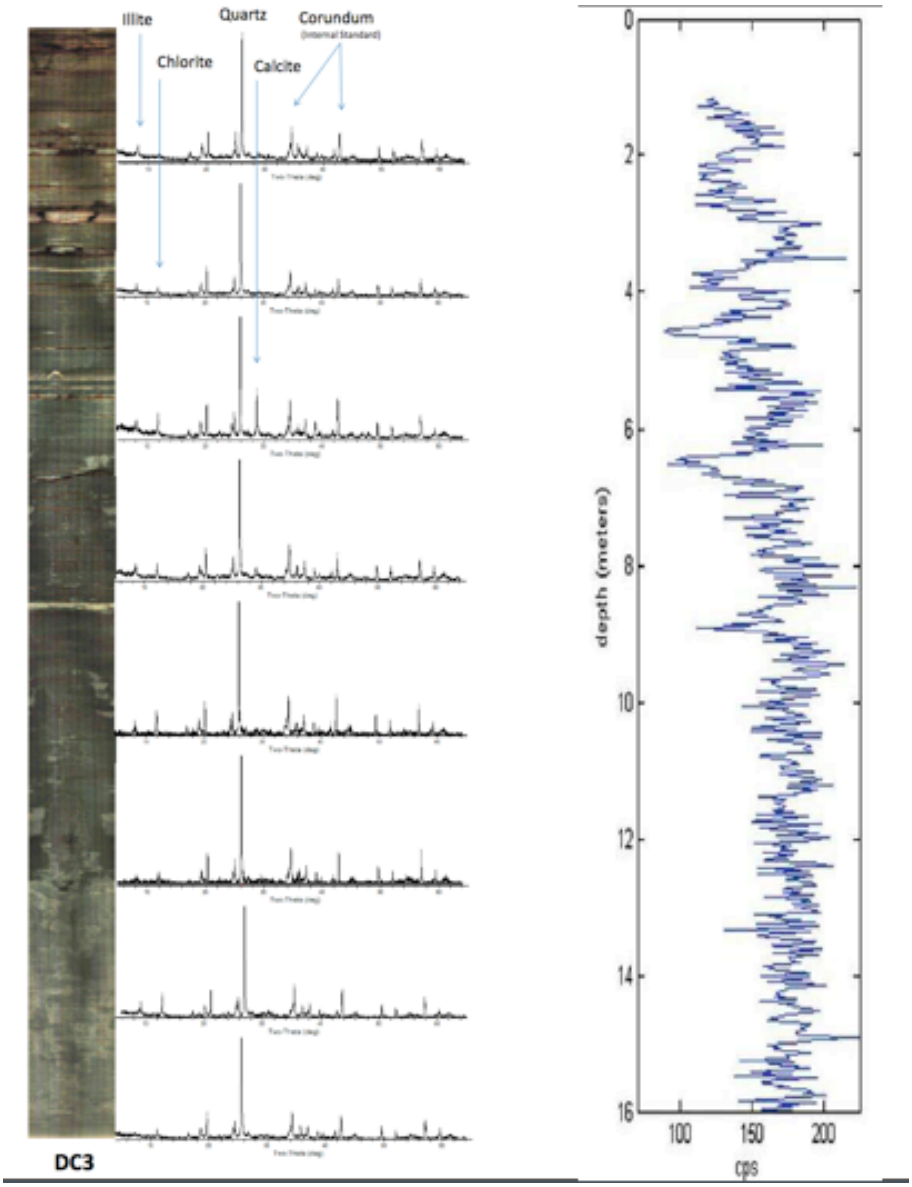

Figure 2: bore hole televiewer images and natural gamma log from DC3, obtained by Dr. Kamini Singha (Geoscience Department, Pennsylvania State University). XRD results are shown adjacent to the depth at which they represent. The carbonate peak seen at 6.4-6.6 meters indicated Ca presence.

2.3 Sample preparation and elemental analysis

Drilled samples were bagged in the field and labeled for appropriate sample depths at DC2, DC3, and DC4 sample sites. All drilled samples were air dried, and the entire bulk sample, consisting of both rock fragments and granular (powders) ground to pass through a 100-mesh sieve (150 μm). Samples were prepared for lithium metaborate fusion according to the methods described by Feldman et al. (1983) to determine bulk chemical analysis by inductively coupled plasma mass spectrometer (ICP-AES) for major elements. Analysis was completed at the Materials Characterization Lab (MCL) at the Pennsylvania State University. The analyses reported with this instrument are estimated to have a precision of +/- 3%. The treatment and procedure of samples from DC2, DC3, and DC4 was identical to sample treatment used for DC1 as previously reported (Jin et al., 2010; Jin et al., 2011).

2.4 XRD analysis

Mineral phases were identified and abundances quantified using x-ray diffraction (XRD). Sample preparation protocol was followed as described by Eberl et al. (2009). All sample preparation steps are intended to maximize random orientation, as to increase the exposed surface area of the included minerals. An internal standard of corundum was used in each sample, to allow quantitative interpretation of XRD peaks. Samples were run on a Scintag 2 PAD-V power x-ray defractometer, scanned from 5 to 65 degrees 2θ, using Cu K-alpha radiation, with a step size of 0.02 degrees 2θ at 1°2θ per minute, and a count time of two seconds (Eberl et al., 2009). XRD patterns were analyzed with JADE mineralogy software, to identify the mineral phases that are present in the samples. RockJock (USGS) mineralogy analysis was additionally run on samples, providing quantitative results on mineral concentrations.

2.5 Sulfur, iron and carbon

Total sulfur concentrations were obtained using a LECO Sulfur Analyzer Coulometer. Roughly 400 mg of sample is weighed into ceramic crucibles combined with tin and iron as combustion additives. The crucible is combusted in an induction furnace, so as to evolve SO_2 gas for detection by titration with the KIO_3 solution. The amount of KIO_3 required to balance the reaction is proportional to the amount of SO_2 evolved. Ferrous iron was measured through titration as described by Goldich et al. (1984). Total ferrous iron concentrations were measured in the laboratory to a precision of +/- 2%. In this study, in particular the transition zone from ferrous (Fe^{2+}) to ferric (Fe^{3+}) iron is identified at 7 m depth in DC3. A USGS shale standard (Cody Shale, SCo-1) was used with every titration to maintain the procedures precision. Total carbon was measured by combustion methods at the Agricultural Analytical Services Laboratory at the Pennsylvania State University, following Nelson et al. (1996) lab protocol. Results are reported as total carbon percentages, including both organic and inorganic carbon.

3.Results

3.1 Major elemental concentrations

Seventeen samples from DC3 drill core were analyzed for major elemental concentrations (Table 1). DC3 generally showed constant Ti, Mn, Si, and Al concentrations with depth, see Figure 3. In contrast, Ca, and Fe were observed to be present at more variable concentrations. For example, samples DC3-8 and DC3-22 have relatively high Ca concentrations at a depth of 2.1-2.3 and 6.4-6.6 meters respectfully. In this study, we assume Zr concentration in the bedrock is not removed or added throughout the profile, i.e., it is an immobile element. Zr is measured with an error of 10 ppm with the ICP-AES technique.

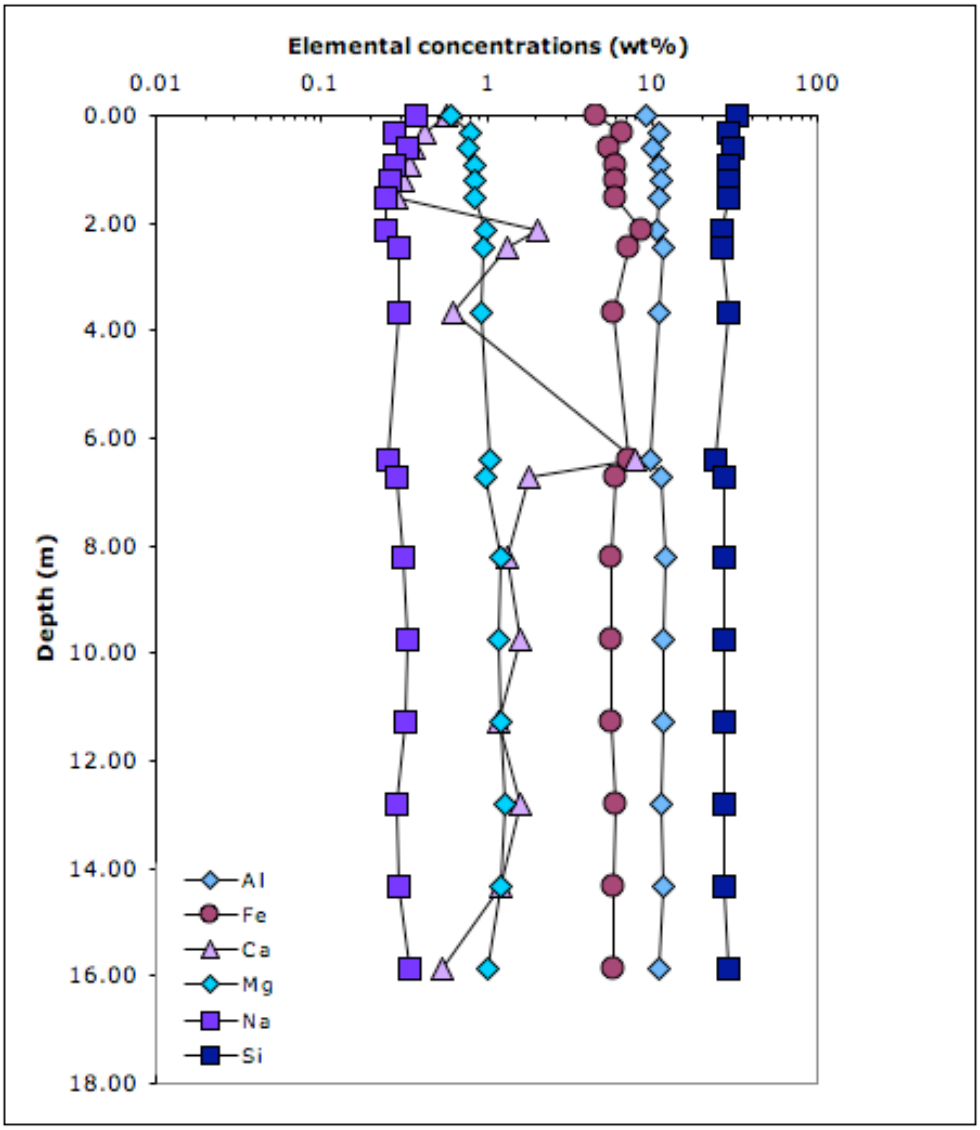

Figure 3: Major element concentrations with depth, measured from the DC3 site. High Ca content is seen at 2.4 and 6.2 meters depth into the bedrock. Al, Fe, Mg, Na, and Si remain relatively constant with depth.

Table 1: Elemental concentrations (wt. %) of drilled samples from DC3-- valley floor of SSHO

Sample ID	Depth range (m)	Al	Ca	Fe	K	Mg	Mn	Na	P	Si	Ti	Zr (ppm)
DC3-1	0-0.3	9.21	0.06	4.64	2.39	0.60	0.17	0.38	0.03	32.4	0.60	280
DC3-2	0.3-0.6	10.9	0.42	6.62	3.56	0.80	0.03	0.28	0.03	29.1	0.59	225
DC3-3	0.6-0.9	10.2	0.37	5.51	3.49	0.77	0.11	0.33	0.04	30.4	0.61	290
DC3-4	0.9-1.2	11.2	0.34	5.95	3.88	0.84	0.14	0.28	0.05	29.0	0.62	230
DC3-5	1.2-1.5	11.3	0.31	6.06	3.98	0.85	0.09	0.26	0.06	28.8	0.63	225
DC3-6	1.5-1.7	11.1	0.28	6.04	3.84	0.86	0.09	0.25	0.05	29.1	0.62	230
DC3-8	2.1-2.3	10.9	2.02	8.75	3.49	0.97	0.38	0.24	0.16	26.2	0.58	175
DC3-9	2.4-2.6	11.7	1.32	7.24	3.92	0.96	0.21	0.29	0.11	26.8	0.61	175
DC3-13	3.6-3.8	11.0	0.62	5.94	3.76	0.93	0.16	0.29	0.07	29.0	0.62	245
DC3-22	6.4-6.6	9.86	8.03	7.20	3.31	1.05	0.20	0.26	0.08	24.4	0.54	185
DC3-23	6.7-6.9	11.3	1.82	6.08	3.99	1.00	0.09	0.29	0.07	27.7	0.61	195
DC3-28	8.2-8.4	11.9	1.34	5.64	4.29	1.22	0.07	0.31	0.06	27.4	0.60	160
DC3-33	9.8-10	11.8	1.59	5.64	4.22	1.19	0.06	0.34	0.02	27.4	0.60	165
DC3-38	11-11.2	11.9	1.20	5.73	4.35	1.23	0.07	0.32	0.06	27.4	0.61	140
DC3-43	13-13.2	11.3	1.57	6.02	4.02	1.30	0.07	0.28	0.04	27.7	0.60	175
DC3-48	14-14.2	11.9	1.23	5.87	4.19	1.23	0.07	0.30	0.05	27.4	0.62	165
DC3-53	15.8-16	11.0	0.53	5.88	3.83	1.00	0.10	0.34	0.04	28.9	0.66	315
Parent[a]		11.5	1.11	5.91	4.09	1.19	0.07	0.31	0.05	27.9	0.63	187

[a]parent concentrations were taken as the average of the deepest seven samples from DC3.

3.2 Mineralogy

Table 2 presents weight percents of minerals for each sample taken at the DC3 site based on RockJock interpretations of X-ray diffractograms. Mineralogy results are consistent with Jin et al. (2010) reporting illite as the dominant clay in the Rose Hill Shale. Of the non-clay members quartz, K-spar and pyrite are generally constant with depth. A significant increase in calcite concentration is observed at depths of 2.1-2.3 and 6.2-6.4 meters interpreted as variation in the bedrock lithology. Kaolinite and vermiculite are present at their highest weight percent within the upper 4 meters of drilled samples, see Figure 4. They are not present at high concentrations with depth.

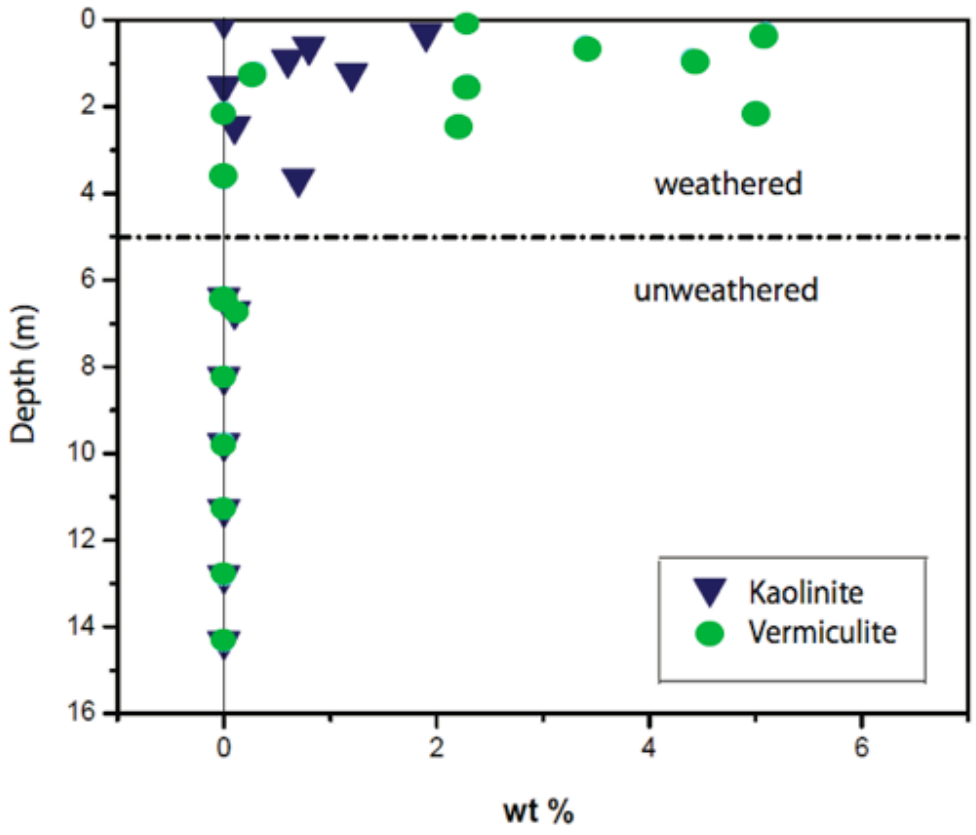

Figure 4: DC3 mineralogy results as obtained by RockJock quantitative program. Kaolinite and vermiculite are only seen in the upper 4 meters of drilled samples. The 4 m dashed line is identified as the illite reaction front. Below 4 m depth, illite has not been weathered.

Table 2: Mineralogy as determined by Quantitative XRD

Sample ID	**Non-Clays**					**Clays**			
	Quartz wt%	K-spar wt%	Calcite wt%	Ankerite wt%	Pyrite wt%	Kaolinite wt%	Illite wt%	Chlorite wt%	Vermiculite wt%
DC3-1	29.0	2.1	0.6	0	0.1	0	55.3	0	2.3
DC3-2	30.9	2.3	0	0	0.2	1.9	43.5	6.2	5.1
DC3-3	36.2	4.5	0.8	0.5	0.2	0.8	50.6	6.0	3.4
DC3-4	29.1	4.9	0.7	0	0.1	0.6	54.9	7.1	4.4
DC3-5	25.8	2.7	0.9	0.3	0.1	1.2	57.2	5.9	0.3
DC3-6	29.0	2.1	0.6	0	0.1	0	55.3	9.5	2.3
DC3-8	24.1	2.5	3.6	0.4	0.3	0	49.7	9.0	5.0
DC3-9	24.2	2.4	2.6	0	0.1	0.1	53.0	11.7	2.2
DC3-13	30.3	2.1	0.6	0.5	0.1	0.7	53.5	11.4	0
DC3-22	24.2	1.3	16.3	1	0.1	0	42.5	12.2	0
DC3-23	26.1	3.5	3.2	0.4	0.1	0.1	50.5	12.5	0.1
DC3-28	25.0	3.1	2.0	2.2	0.1	0	54.1	13.5	0
DC3-33	25.3	2.4	2.1	1.8	0.1	0	53.1	14.2	0
DC3-38	25.5	3.6	1.5	1.6	0.2	0	50.4	4.5	0
DC3-43	26.3	3.1	1.1	2	0.3	0	47.5	9.1	0
DC3-48	27.7	3.0	1.3	1.5	0.1	0	49.3	10.6	0
DC3-53	30.1	3.3	0	1.4	0.2	0	43.9	14.2	0

*All weight percents were normalized to 100, as determined from running XRD patterns on RockJock mineralogy analysis program (USGS) following the protocol reported in Eberl (2009). RockJock determines mineralogy wt % within 4% error (2 standard deviations).

3.3 Ferrous iron

Ferrous iron titrations reveal that Fe^{2+} was depleted in shallow samples, above 7 meters depth. Using the total Fe elemental percents obtained from ICP-AES, ferrous iron [Fe^{2+}] was subtracted from Fe_{Total} to yield ferric iron [Fe^{3+}] concentrations with depth. This calculation assumes,

$$[Fe^{2+}] + [Fe^{3+}] = Fe_{Total} \quad (1)$$

with no additional Fe inputs to the system. Table 3 reports Fe^{2+} and Fe^{3+} concentrations with depth into bedrock, in the valley floor site (DC3).

Table 3: Ferrous Iron concentration, samples analyzed from drill core DC3 site*

Sample ID	Fe_{Total} wt%	$Ferrous^{2+}$ wt%	$Ferric^{3+}$ wt%
DC3-3	5.52	0.97	4.54
DC3-5	6.06	1.15	4.91
DC3-8	7.24	1.42	5.82
DC3-13	5.94	2.19	3.74
DC3-22	7.20	3.52	3.68
DC3-23	6.08	2.87	3.21
DC3-28	5.64	4.94	0.70
DC3-33	5.64	4.74	0.89
DC3-38	5.74	4.66	1.07
DC3-43	6.02	5.44	0.59
DC3-48	5.87	4.90	0.97
DC3-53	5.88	3.79	2.09

* The uncertainty for both ferrous iron titrations and total iron is +/- 5%

3.4 Sulfur-Pyrite

The S analysis documents the concentration of total S in the sample. Given the mineralogy (Table 2) and other observations of pyrite (Jin et al., 2011) all S detected in the samples is attributed to pyrite. As documented in Table 4, a pyrite depleted zone is observed from 0 to 7 meters depth, within the valley floor of the catchment (DC3). Below this zone, 8-15 meters pyrite is preserved within the bedrock. Pyrite is detected in concentrations ranging from 1644 to 2279 ppm.

Table 4: pyrite concentration, analyzed from drill core DC3 site.

Sample ID	pyrite (ppm)	$\tau_{i,j}$
DC3-2	126	-0.91
DC3-3	117	-0.92
DC3-8	139	-0.84
DC3-13	111	-0.91
DC3-22	135	-0.85
DC3-28	1813	1.18
DC3-33	1963	1.29
DC3-38	2279	2.13
DC3-43	2272*	1.50
DC3-48	1644	0.92
DC3-53	1763*	0.08

* samples were run multiple times for machine accuracy, the average is reported.

3.5 Water table

Water movement through the bedrock is a significant control on the dissolution and precipitation of mineral species (White et al. 2008). During the driest months in the catchment, depth to water table was measured in August 2010 to be an average of 3.25 meters in the valley floor (Holmes, 2010) reported in Table 5 with well locations shown on Figure 5. During the wet winter and fall seasons when there is water flow in the 1D stream, the water table is recorded as being at the ground surface in the valley floor (0 meters). Therefore in 2010 it was documented the water table fluctuates no more than 3 meters from the driest to wettest months in the catchment. The bulk percentage of water table measurements were taken in 2010, however not to disregard the fluctuation of water table depth from year to year. It is not unreasonable to assume in drier years, depth to water table may have been significantly deeper than the values reported in 2010.

The water table lies much deeper at the ridge top, DC1 site. Measurements taken in April of 2011 report a perched water table at the ridge top. A difference was measured of an average of 7 meters between Well DC0 and DC1. The two wells are located at the same elevation <10 meters apart at the ridge top site at SSHO. The shallower depth to water table was measured at DC0 to be 17.6m, and DC1 to be 24.2 meters. It has been hypothesized the lithology of the underlying bedrock is the source of the inconsistent depth to water table at the ridge top. The understanding behind the perched water table at the ridge top is still unclear.

Table 5: SSHO water table summary, depth to water table measurements taken in 2010, and 2011*

Month, 2010	Depth to water table (m)				
	Well 4	Well 5	Well 7	Well 12	Well 17
April	0.63	1.93	1.21	--	--
May	0.60	1.88	1.20	--	--
August	1.01	2.15	1.28	3.15	1.64
September	0.85	2.11	1.21	3.20	1.64
October	0.73	2.08	1.18	3.20	1.71
November	0.67	2.05	1.07	3.23	1.62
Month, 2011	Depth to water table (m)				
	Well 11	Well 9	DC3	DC1	DC0
February	0.03	4.11	0.84	--	17.5
March	0.05	4.53	0.45	--	19.4
April	--	--	--	24.2	17.6

*2010 data was collected by George Holmes, Civil Engineering, The Pennsylvania State University. Well ID's are supplemented with Figure 5, a map of SSHO showing Well locations.

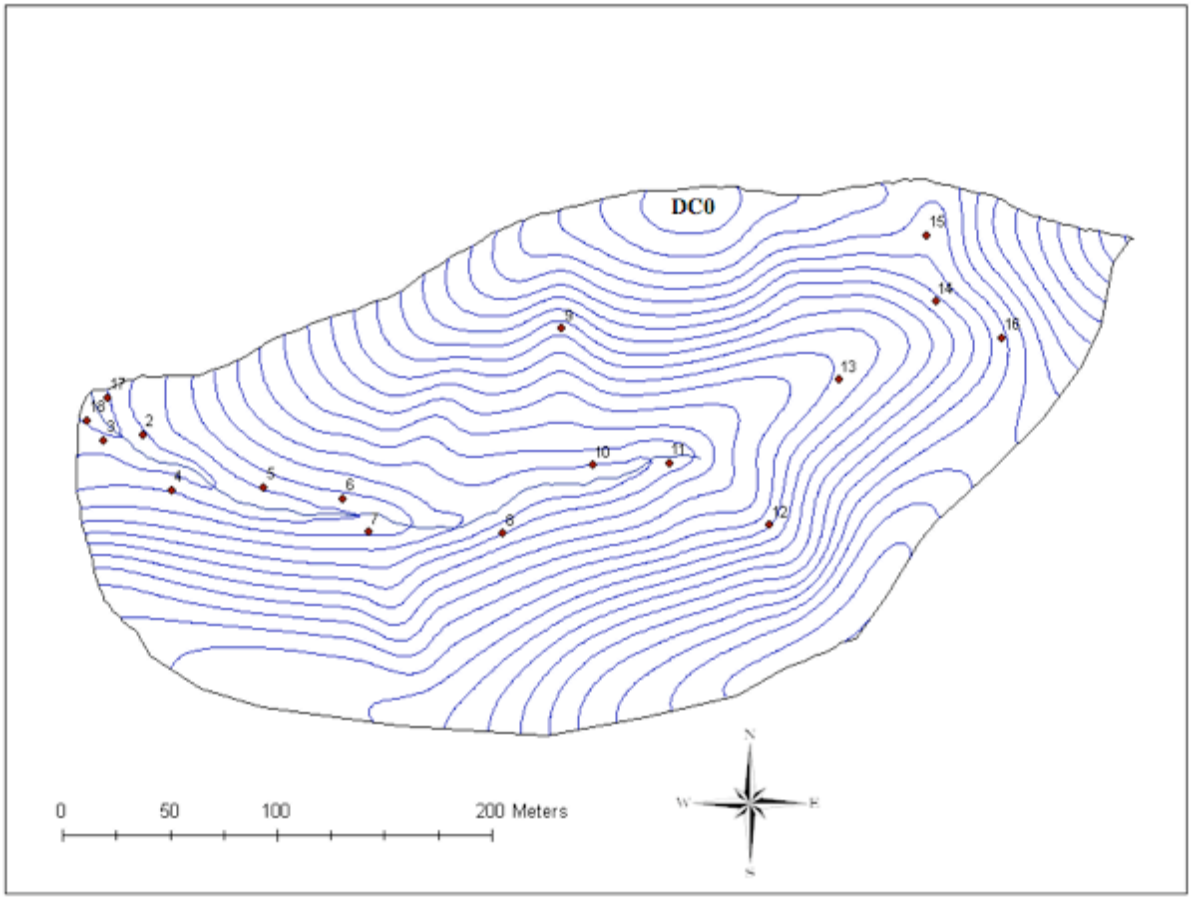

Figure 5: Map of SSHO well ID numbers and locations, to supplement water table Table 5. Map was created and wells were drilled by Chris Duffy's research group, Department of Civil Engineering, The Pennsylvania State University. The authors would like to thank George Holmes, Masters Student in Chris Duffy's research group, Department of Civil Engineering for assistance with water table data, and maps.

4. Discussion

4.1 Parent shale classification

At the DC3 site, samples consistently ranged from brown color in shallow depths, to dark grey color in deeper samples; a sharp transition from brown to grey is noted between 6.9 and 8.2 meters. Additionally a sharp change from wet to dry samples is noted between 2.6 and 3.6 meters the depth representative of the summer water table. When classifying the parent bedrock composition, we discussed two different assumptions. First, the average of all samples (every depth) was used as parent, similarly done in Jin et al. (2010). However it was noted DC3 elemental composition was much more variable with depth than DC1 reported in Jin et al. (2010), and taking the average of the entire core was not accurate parent composition. It was determined the ridge top (DC1) parent was not an accurate representation of the valley floor (DC3) parent due to the steep dip of the bedrock. Second, the parent bedrock composition was determined by averaging the seven deepest samples from DC2, DC3, and DC4 valley floor drilled samples. All three drill cores at the valley floor sites are closely spaced, no more than 5 meter apart therefore we assume the lithology is consistently the same in all three valley floor wells. However with further analysis it has been hypothesized the deepest most sample in DC2, DC3, and DC4 (15 m) is of the Keefer Sandstone, and therefore was removed from the parent composition used in this study.

4.2 Geochemical reaction fronts

In this study we assume Zr is essentially immobile within the catchment, which was observed in the DC1 core as well (Jin et al., 2010). Although Ti and Zr are both assumed immobile in the parent bedrock, Zr is preferably used in this study as the immobile element. The

relative gain and loss of elements as a function of depth in bedrock can be calculated using the mass transfer coefficient τ, according to the following equation (Brimhall and Dietrich, 1987; Anderson et al., 2002):

$$\tau_{i,j} = \frac{C_{j,w}}{C_{j,p}} \frac{C_{i,p}}{C_{i,w}} - 1 \qquad (2)$$

Positive $\tau_{i,j}$ values indicate enrichment of the element of interest *j* in soils or rock (w), with respect to the immobile element *i*, of the parent (p). Negative $\tau_{i,j}$ values indicate depletion of the element of interest with respect to the parent (Anderson et al., 2002). Therefore values of zero indicate no change of the element of interest with respect to the parent, and values of -1 indicate total depletion. Table 6. reports τ values for DC3 samples, with Zr as the immobile element.

In this study the term *reaction front* is defined by the upper limit of the enriched zone of a chemical profile. More specifically the upper boundary is set by the first enriched data point in a profile with respect to parent concentration. The lower boundary of the reaction front is set by the first data point returning to parent composition, with depth. Within the upper and lower boundary conditions, is termed the reaction front of the chemical species. When we observe depletion, such as with [Ca] the depletion profile is said to end at the first point returning to parent composition.

i.) Carbonate

In DC3, major elements such as Si, Na, Mn, Mg, and Al remain constant with depth. The Ca enrichment observed most prominently at 6.2 meters is associated with i) carbonate weathering, ii) lithological heterogeneity, or iii) both. It would be expected that lithological heterogeneities can cause variations in [Ca] with depth, and may be attributed to the high levels

of [Ca] seen in the bedrock, especially at 6 m as reported by Figure 6a. On the other hand, we observe an almost complete depletion of [Ca] presence in the upper 3 m in the valley floor sites, DC2, DC3, DC4 as reported by Figure 6b. This leads us to term 3 meters in the valley floor as the base of the carbonate reaction front. We are inferring the flow of meteoric water is dissolving away any [Ca] present in the upper 3 meters of bedrock. Therefore, the large variations in [Ca] at depth are attributed to lithogical heterogeneity, contrasted with the complete depletion of [Ca] from 0-3m as being attributed to dissolution. This depletion is also observed in the upper 25 m of DC1 at the ridge top. Furthermore allowing us to correlate the carbonate reaction front from ridge top to valley floor, and essentially throughout the entire catchment.

XRD analysis on DC3 samples is in agreement with findings from Jin et al. (2010) in which the calcite is reported as ankerite—an Fe rich calcium carbonate member [$Ca(Fe,Mg,Mn)(CO_3)_2$]. Calcite is depleted from the surface to a depth of 3 meters, as indicated by values of $\tau < 1$. From 3 to 7 meters in the valley floor Ca is enriched, in relation to the parent bedrock as seen in all three valley floor sites (DC2, DC3, DC4). Below 7 meters Ca returns to parent concentration, zero on the τ scale. Factors explaining this may tie to both present and past water table behavior. Kuntz et al. (2010) attributes this Ca rich zone at 6 meters with a slow drilling zone, in which they labeled the depth as a transition from highly-weathered shale to less-weathered shale.

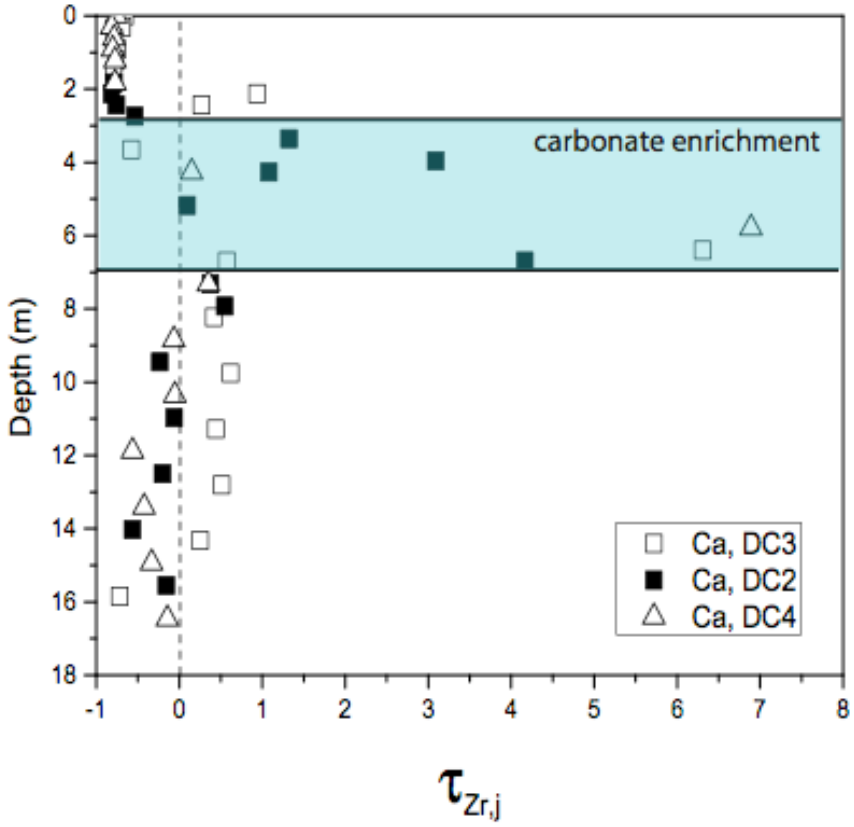

Figure 6a: carbonate enrichment is seen ranging from 3-7 meters depth into bedrock at all three valley floor sites (DC2, DC3, DC4). Values are expressed as τ, with Zr as the immobile element. At parent bedrock $\tau = 0$. Therefore where $\tau > 1$ the element of interest, Ca is assumed to be enriched with respect to parent bedrock. When $\tau < 1$, Ca is depleted with respect to parent, seen from 0-3 meters in the above profile.

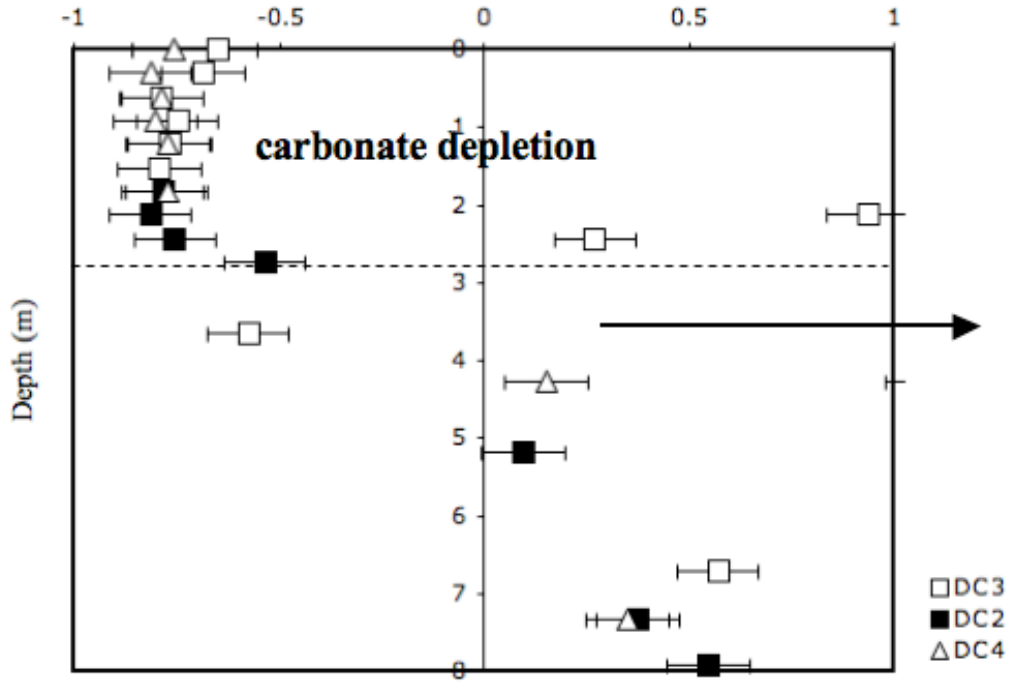

Figure 6b: carbonate enriched τ values were permitted to go off scale as indicated by the balck aarow. The depletion front is zoomed in as to see the signifcance of [Ca] depletion within the upper 3 meters of all three valley floor drill cores, DC2, DC3, DC4.

ii.) Pyrite

It was assumed that S detected by chemical analysis was present as pyrite in the shale. Pyrite oxidation fronts are typically driven by presence of oxygen in meteoric fluids, and are often catalyzed by microbial activity. Oxygen concentrations can often be correlated to the permanent or temporary water table, on the catchment scale. Hercod et al (1998) suggest that pyrite dissolution is irreversible and insensitive to seasonal changes such as temperature, precipitation and organic activity and instead theorize the redox front represents the gradual movement of the pyrite weathering with depth. Drake et al. (2009) defines the depth at which complete oxidation of pyrite is observed as the position of the redox front in the bedrock. That is, below the redox front there exists a transition zone from oxidizing to reducing conditions. Pyrite concentration with depth in DC3 shows depletion, $\tau < 0$ from 0-7 meters depth as reported in Figure 7. 8-15 meters depth contrastingly shows enrichment of pyrite in samples, $\tau > 0$. The weathering of bedrock has dissolved any sulfur (pyrite) bearing minerals in the upper most 7 meters. Within the reaction front of 8-15 meters, pyrite is preserved. The deepest sample appears to return to parent concentration.

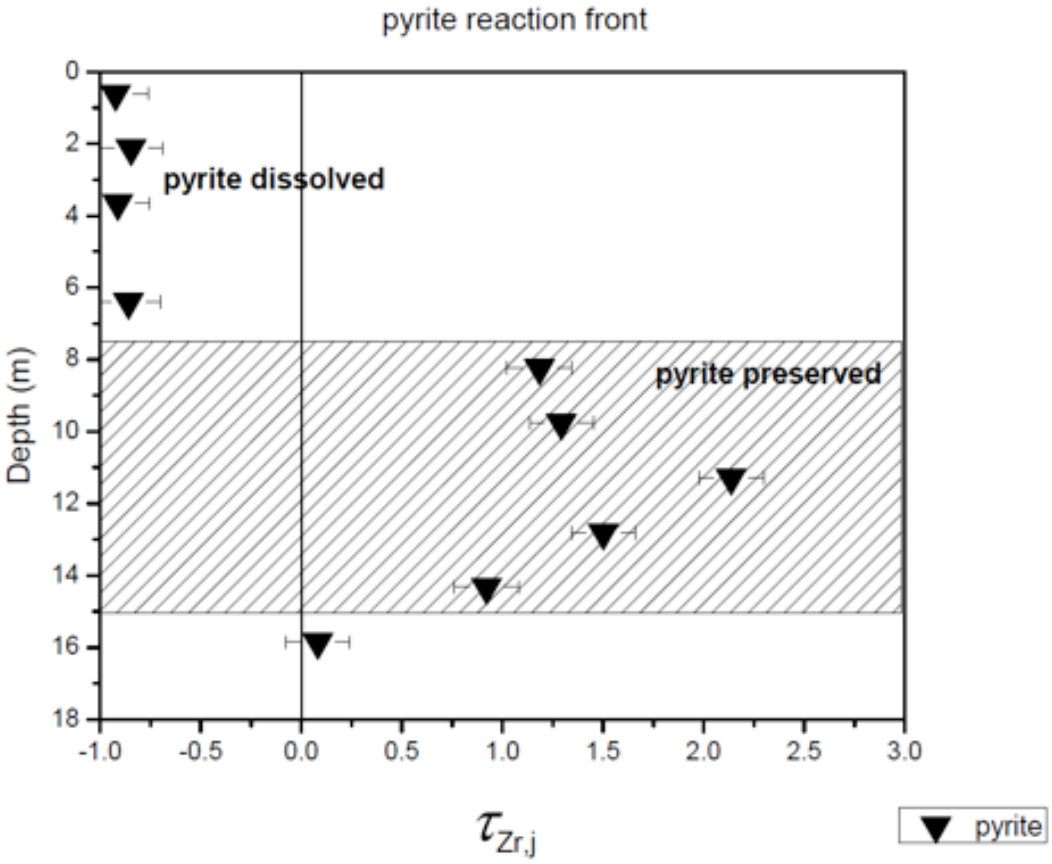

Figure 7: Pyrite concentration with depth in DC3 shows depletion, $\tau < 0$ from 0-7 meters depth. 8-15 meters depth contrastingly shows enrichment of pyrite in samples, $\tau > 0$. The weathering of bedrock has dissolved any sulfur (pyrite) bearing minerals in the upper most 7 meters. Within the reaction front of 8-15 meters, pyrite is preserved.

iii.) Ferrous-ferric

Ferrous iron titrations in DC3 reveal a transition from ferrous iron (Fe^{2+}) to ferric iron (Fe^{3+}) at a depth of 7 meters as reported in Figure 8. Enrichment of ferric and depletion of ferrous above 7 meters, with enrichment of ferrous and depletion of ferric below 7 meters. Jin et al. (2011) reports this Fe reaction front at 25 m below the ridge top site (DC1). It is hypothesized the depth of 7 m in valley floor and 25 m at the ridge top is the same zone in which ankerite is present. The iron end-member of ankerite oxidizing Fe^{+2} to Fe^{3+} would serve to consistently explain the high levels of Ca, in addition to the oxidation state of iron with depth. The depth of 7 m where we observe this transition from Fe^{+2} to Fe^{3+} is the same depth at which we observe the initial presence of pyrite in DC3. Therefore the change in redox conditions as seen by the iron transition in the bedrock correlates with the presence of pyrite.

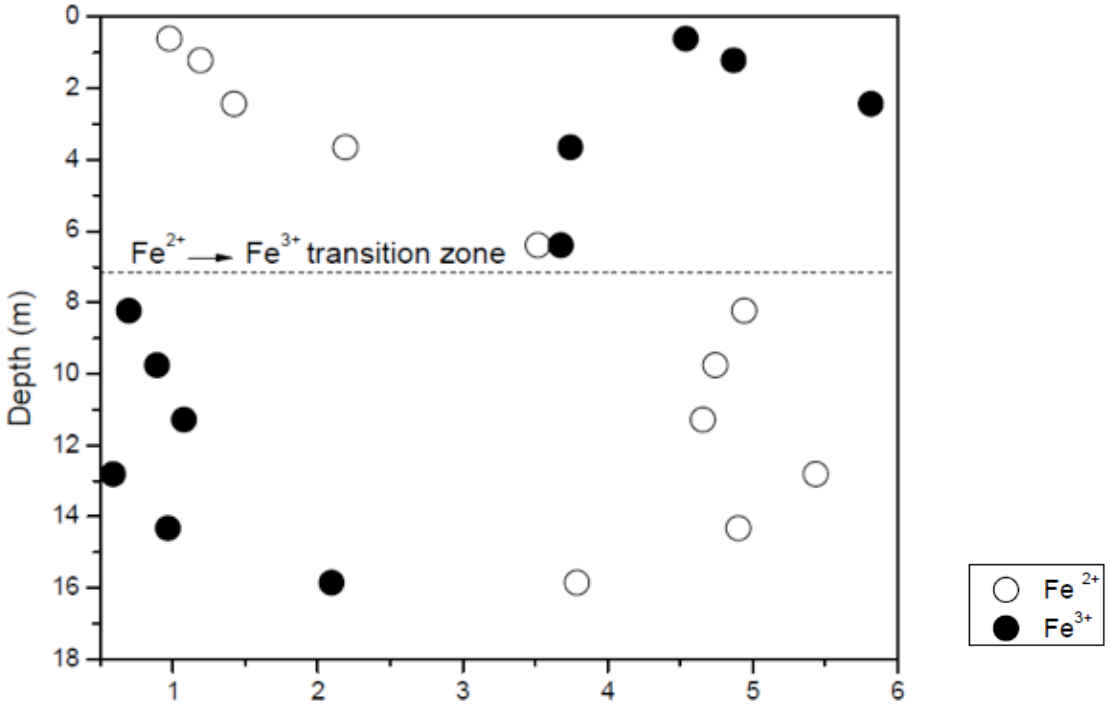

Figure 8: Ferrous iron titrations in DC3 reveal a transition from ferrous iron (Fe^{2+}) to ferric iron (Fe^{3+}) at a depth of 7 meters. Enrichment of ferric and depletion of ferrous above 7 meters, with enrichment of ferrous and depletion of ferric below 7 meters. This transition is hypothesized as representing the depth at which the Fe^{2+} end member in ankerite is oxidized to Fe^{3+}.

iv.) Illite

From XRD and mineralogy results we have determined illite to be the dominant clay member in the Rose Hill Shale, underlying SSHO. The weathering of illite produces secondary mineral phases such as kaolinite and vermiculite. Kaolinite and vermiculite are formed as a weathering products of illite, therefore we infer their presence is evidence of weathering. We used this mineralogy to identify depths at which illite is weathering from the regolith into bedrock. It was determined illite weathering front extends to 4 meters depth in the valley floor (DC3) and 0.5 meters at the ridge top (DC1). Illite is the only weathering front in which we see a deeper extent in the valley floor than ridge top. This trend is thought to be mirroring the soil thickness in the catchment. We observe thinner soils (<0.5 m) at the ridge top and thicker soils in the valley floor of the catchment (< 2 m). Illite weathering drives the disaggregation of bedrock, therefore controlling soil thickness by its weathering front.

Table 6: DC3 Tau values, with Zr as an immobile element ($\tau_{Zr,j}$)

Sample ID	Depth range (m)	Al,$\tau_{Ti,j}$	Ca,$\tau_{Ti,j}$	Fe,$\tau_{Ti,j}$	K,$\tau_{Ti,j}$	Mg,$\tau_{Ti,j}$	Mn,$\tau_{Ti,j}$	Na,$\tau_{Ti,j}$	P,$\tau_{Ti,j}$	Si,$\tau_{Ti,j}$
DC3-1	0-0.3	-0.46	-0.65	-0.48	-0.61	-0.66	0.74	-0.19	-0.52	-0.22
DC3-2	0.3-0.6	-0.21	-0.68	-0.07	-0.28	-0.44	-0.58	-0.26	-0.50	-0.13
DC3-3	0.6-0.9	-0.43	-0.79	-0.40	-0.45	-0.58	0.04	-0.32	-0.49	-0.30
DC3-4	0.9-1.2	-0.21	-0.75	-0.18	-0.23	-0.43	0.73	-0.28	-0.11	-0.16
DC3-5	1.2-1.5	-0.18	-0.77	-0.15	-0.19	-0.41	0.14	-0.31	0.068	-0.14
DC3-6	1.5-1.7	-0.22	-0.79	-0.17	-0.24	-0.41	0.10	-0.35	-0.21	-0.15
DC3-8	2.1-2.3	-0.01	0.94	0.58	-0.09	-0.13	5.20	-0.16	2.60	-0.03
DC3-9	2.4-2.6	-0.09	0.27	0.31	0.02	-0.14	2.43	-0.01	1.50	0.03
DC3-13	3.6-3.8	-0.27	-0.57	-0.23	-0.30	-0.41	0.82	-0.28	0.14	-0.21
DC3-22	6.4-6.6	-0.13	6.31	0.23	-0.18	-0.11	2.00	-0.17	0.73	-0.11
DC3-23	6.7-6.9	-0.06	0.57	-0.01	-0.06	-0.20	0.33	-0.12	0.44	-0.05
DC3-28	8.2-8.4	-0.21	0.42	0.11	0.23	0.20	0.29	-0.16	0.59	0.15
DC3-33	9.8-10	-0.16	0.62	0.08	0.17	0.13	0.12	-0.22	-0.45	0.11
DC3-38	11-11.2	-0.38	0.44	0.29	0.42	0.38	0.33	-0.38	0.71	0.31
DC3-43	13-13.2	-0.05	0.51	0.09	0.04	0.17	0.20	-0.03	-0.16	0.06
DC3-48	14-14.2	-0.17	0.25	0.13	0.16	0.17	0.13	0.08	0.34	0.11
DC3-53	15.8-16	-0.43	-0.72	-0.41	-0.44	-0.50	-0.06	-0.34	-0.49	-0.38
Parent [a], $C_{i,p}$		11.47	1.109	5.910	4.086	1.192	0.066	0.312	0.047	27.90

[a] Parent values were determined as an average of the 7 deepest samples from the drill cores DC2, DC3, and DC4

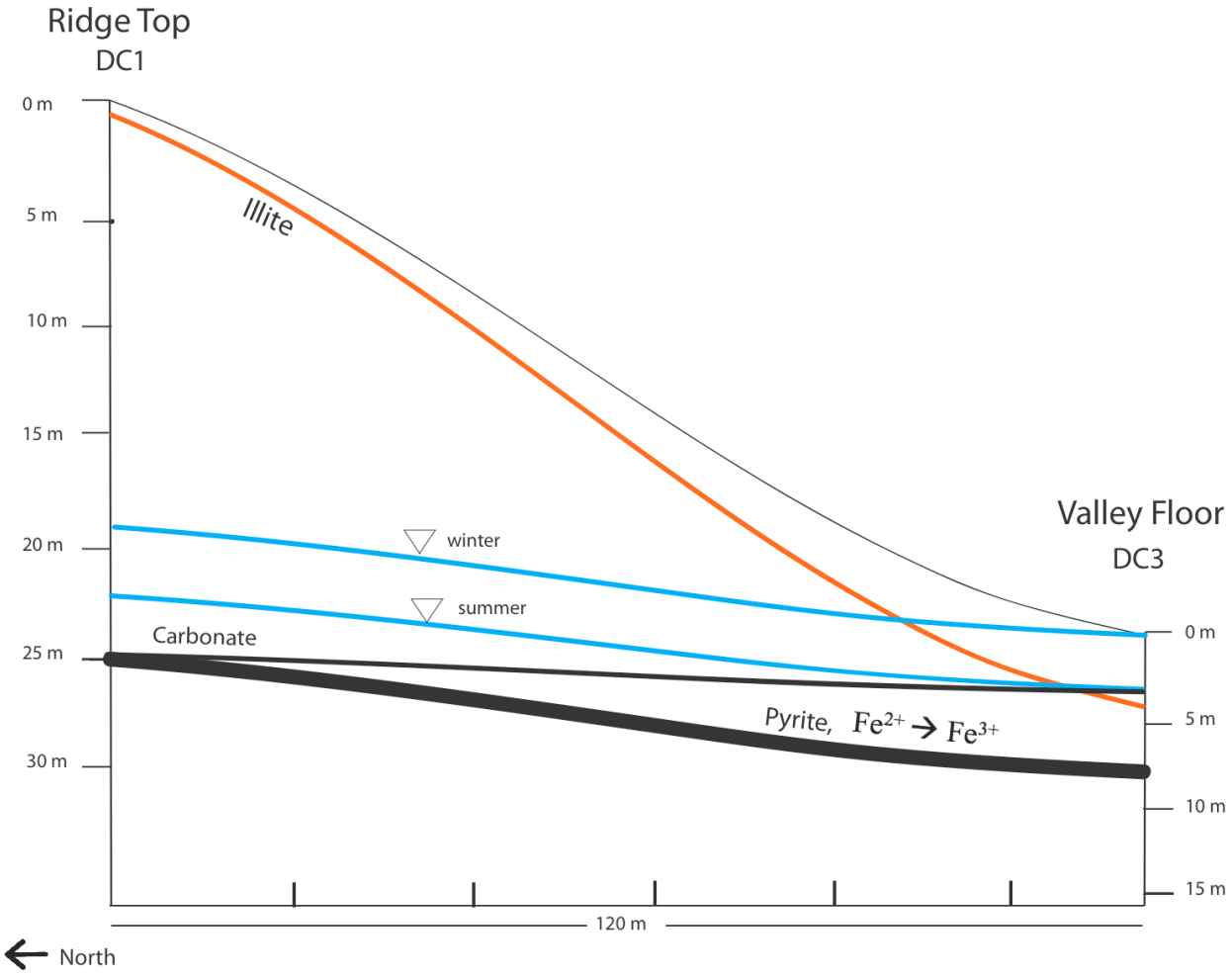

Figure 9: Geochemical reaction fronts are correlated between the valley floor site (DC3) and the ridge top site (DC1) within the catchment. Blue lines represent averaged summer and winter water table depths. A pyrite reaction front is observed at 7 meters depth in the valley floor, and 25 meters at the ridge top. A carbonate depletion front is noted at 3 meters depth in the valley floor, and 25 meters at the ridge top. Additionally a $Fe^{2+} \rightarrow Fe^{3+}$ transition depth is observed at 7 meters depth in the valley floor and 25 meters at the ridge top site. The illite weathering front is the only front seen at shallower depths at the ridge top, and deeper in the valley floor. Illite weathering front is observed at 4 m in the valley floor and 0.5m at the ridge top.

4.3 XRD

The clay mineralogy is dominantly composed of illites and chlorites, with some integrated vermiculites and kaolinites. Vermiculites and kaolinites are present in shallow samples, and depleted with depth. The kaolinite and vermiculite detected by XRD are used to track the illite weathering front within the upper drilled samples from the valley floor. Illite shows depletion within the uppermost 4 meters in DC3, returning to parent composition with depth. The majority of the non-clay counterparts is quartz, k-spar, and some calcite. XRD and chemical analysis has suggested the calcite detected in the bedrock may be classified as ankerite, Fe-rich calcite [$Ca(Fe, Mg, Mn)(CO_3)_2$]. An unusually high Ca concentration is associated with a Ca rich zone in the lithology, detected at 6 m depth. Quartz concentration remains constant with depth in DC3.

4.4 Gamma ray

Following the drilling of DC3 along with tele-viewer images, natural gamma ray in counts per second were measured in the drill core site as reported in Figure 2. Kuntz et al. (2010) labeled 6 m depth as a slow drilling zone. This zone was interpreted as a transition from highly weathered bedrock to less weathered bedrock. Additionally, low gamma rays in the upper 7 m of the DC3 were attributed to removal of clay-rich materials (Kuntz et al. 2010). The low gamma counts at 6 m may represent the loss of clay minerals, which is consistent with the other results of this study. Multiple reaction fronts are recognized in the 6-8 m range in DC3, therefore the change in gamma is in agreement with the intensification of bedrock weathering at this depth.

5. Conclusions

Our analysis of the extent of deep shale weathering at SSHO has yielded several important findings. Most importantly, we have determined and identified the presence of mineral reactions well beneath the regolith and into bedrock. We can report with confidence that shale weathering extends into bedrock at depths of 7 m at the valley floor and 25 m at the ridge top in SSHO. Based on geochemical and mineralogical characterizations, weathering fronts were identified in drilled samples from the valley floor. Seventeen samples from a 16 meter deep drill core taken at the valley floor site were analyzed and compared to similar samples from the ridge top. A carbonate weathering front was identified at 3 m depth, an illite weathering front at 4 m depth, and a pyrite oxidation front and ferrous-ferric transition at 7 m depth in the valley floor of SSHO. Identical reaction fronts were identified at the ridge top of the SSHO catchment, although at variable depths. Ridge top carbonate weathering front is noted at 25 m, pyrite oxidation front an ferrous-ferric transition at 25 m and illite weathering front at 0.5 m (Figure 9).

We have concluded the water table within the catchment is controlling the [Ca] depletion in the valley floor. The large variations in [Ca] at depth are attributed to lithogical heterogeneity, contrasted with the complete depletion of [Ca] from 0-3m as being attributed to dissolution. Both the pyrite reaction front and iron redox front fall at 7 m in the valley floor. Representing the depth at which redox conditions change from favoring oxidizing conditions above 7 m and into conditions favoring reduction below 7 m. With the exception if illite we see reaction fronts at consistently shallower depths in the valley floor in comparison to the ridge top. The illite weathering front is noted at 4 m in the valley floor and 0.5 m at the ridge top. The illite weathering front depth mimics soil thickness within the catchment, in that the ridge top has shallower soils than in the valley floor. Efforts should be continued to further understand the

processes of deep shale weathering on the catchment scale, as well as the linkage between deep shale weathering and water table relationships within SSHO.

REFERENCES

Anderson, S. P., von Blanckenburg F. and White A. F. (2007) Physical and chemical controls on the Critical Zone. *Elements* 3, 315-319.

Brantley, S.L., White T.S., White A.F., Sparks D., Richter D., Pregitzer K., Derry L., Chorover J., Chadwick O., April R., Anderson S., Amundson R., (2006) Frontiers in exploration of the critical zone, an NSF-sponsored workshop. *National Science Foundation*. 30 pp

Brimhall, G. H. and Dietrich W. E. (1987) Constitutive mass balance reactions between chemical composition, volume, density, porosity, and strain in metosomatic hydrochemicalsystems: results on pedogenesis. *Geochim. Cosmochim. Acta*. 51, 567-587.

Drake, H., Tullborg, E., MacKenzie, A.B. (2009) Detecting the near-surface redox front in crystalline bedrock using fracture mineral distribution, geochemistry and U-series disequilibrium. Applied Geochemistry. 24, 1023-1039.

Eberl, D.D., and Smith, D.B., (2009) Mineralogy of soils from two continental-scale transects across the United States and Canada and its relation to soil geochemistry and climate. *Applied Geochemistry*. 24, 1394-1404.

Eberl, D.D. (2009) User's guide to RockJock— A program for determining quantitative mineralogy from powder x-ray diffraction data. The United States Geological Survey. Open file report 03-78.

Feldman, C. (1983), Behavior of Trace Refractory Minerals in the Lithium Metaborate Fusion Acid Dissolution Procedure, Anal. Chem., Vol 55, No. 14, 2451-2453

Fold, R. L. (1960) Petergraphy and origin of Tuscarora Rose Hill, and Keefer formations, Lower and Middle Silurian of eastern west Virginia. *J. Sed. Petrol*. 30, 1-58.

Goldich, S.S., (1984) Determination of ferrous iron in silicate rocks. *Chemical Geology*. 42, 343-347.

Hercod, D.J., Brady, P.V., and Gregory, R.T. (1998) Catchment-scale coupling between pyrite oxidation and calcite weathering. Chemical Geology. 151, 259-276.

Hoskins, D. M. (1976) Pine Grove Mills Quadrangle Pennsylvania (7.5 min series, topographic). This map is from Map 61-Atlas of Preliminary Geologic Quadrangle maps of Pennsylvania 1981, PA Geological Survey.

Kuntz, B. W., Singha, K., Brantley, S. L., Gooseff., M. N., Parizek, R. R. (2010) Laboratory, field, and modeling analysis of solute transport behavior at the Shale Hills Critical Zone Observatory. MS Thesis Defense. Pennsylvania State University, University Park, PA.

Jin, L., Rother, G., Cole, D. R., Mildner, D. F. R., Duffy, C. J., Brantley, S. L. (2011) Characterization of deep weathering and nanoporosity development in shale- a neutron study. American Mineralogist. 96, 498-512.

Jin, L., R. Ravella, B. Ketchum, P. R. Bierman, P. Heaney, T. White, and S. L. Brantley. (2010): Mineral weathering and elemental transport during hillslope evolution at the susquehanna/shale hills critical zone observatory. *Geochimica Et Cosmochimica Acta* 74, 3669-691.

Lin, H.S., Kogelmann W., Walker C., and Burns M.A. (2006) Soil moisture patterns in a forested catchment: A hydropedological perspective. *Geoderma*. 131, 346-348.

Lynch, J. A. (1976) Effects of antecedent soil moisture on storm hydrographs. PhD Dissertation. Pennsylvania State University, University Park, PA.

Nelson, D.W. and L.E. Sommers. (1996). Total Carbon, Organic Carbon, and Organic Matter. P 961-1010. In D.L. Sparks (ed). Methods of Soil Analysis, Part 3. Chemical Methods. Soil Science Soceity of America Book Series Number 5. American Society of Agronomy, Madison, WI.

Riebe, C.S, Kirchner, J.W, and Finkel, R.C. (2003) Long-term rates of chemical weathering and physical erosion from cosmogenic nuclides and geochemical mass balance. *Geochim. Cosmochim. Acta* 67, 441-4427.

Tuttle, L.W, Breit, G.N., (2009) Weathering of the New Albany Shale, Kentucky, USA: I Weathering zones defined by mineralogy and major-element composition. Applied Geochemistry. 24, 1549-1564.

White A. F., (2008) Quantitative approaches to characterizing natural chemical weathering rates. In *Kinetics of Water-Rock Interaction*. (eds. S. L. Brantley, J. D. Kubicki and A. F. White). Springer, New York, pp. 469-544.

APPENDIX

Table 7: Elemental concentrations (wt%) of drilled samples from DC2-- valley floor of SSHO

Sample Depth ID	Al	Ca	Fe	K	Mg	Mn	Na	P	Si	Ti	Zr (ppm)
DC2 6-7	11.70	0.26	6.03	4.15	0.91	0.06	0.27	0.05	28.38	0.65	205
DC2 7-8	11.48	0.25	5.92	3.92	0.94	0.10	0.35	0.03	28.71	0.63	230
DC2 8-8.5	12.01	0.28	5.97	4.19	1.00	0.07	0.33	0.05	27.97	0.65	190
DC2 9-9.5	11.00	0.62	5.54	3.82	0.95	0.07	0.32	0.05	29.20	0.65	225
DC2 11-13	10.98	3.04	5.08	3.79	0.93	0.10	0.37	0.04	27.93	0.63	220
DC2 13-14	10.40	4.86	6.10	3.59	1.02	0.13	0.31	0.05	26.65	0.60	200
DC2 14-15	11.47	2.22	6.24	4.04	1.07	0.07	0.30	0.04	27.08	0.62	180
DC2 17-18	11.60	1.27	5.95	4.11	1.12	0.11	0.33	0.05	27.69	0.60	195
DC2 22-23	9.16	7.52	5.75	3.18	1.35	0.19	0.30	0.06	26.21	0.54	245
DC2 24-25	10.96	1.84	6.48	3.80	1.27	0.11	0.30	0.04	27.62	0.59	225
DC2 26-27	11.50	1.84	6.47	3.99	1.27	0.08	0.33	0.04	27.01	0.62	200
DC2 31-32	11.79	0.77	6.00	4.15	1.20	0.06	0.33	0.05	27.72	0.64	170
DC2 36-37	11.88	0.95	5.73	4.33	1.20	0.06	0.35	0.04	27.58	0.66	170
DC2 41-42	11.35	0.90	5.86	3.98	1.13	0.05	0.32	0.04	28.27	0.68	190
DC2 46-47	11.63	0.47	5.88	4.17	1.17	0.03	0.33	0.05	28.14	0.67	180
DC2 51-52	10.32	1.16	5.76	3.54	1.12	0.06	0.28	0.05	29.43	0.57	230
Parent[a]	11.5	1.11	5.91	4.09	1.19	0.07	0.31	0.05	27.9	0.63	187

[a]parent concentrations were taken as the average of the deepest seven samples from DC2.

Table 8: Elemental concentrations (wt%) of drilled samples from DC4-- valley floor of SSHO

Sample ID	Al	Ca	Fe	K	Mg	Mn	Na	P	Si	Ti	Zr (ppm)
DC4 0-1	10.74	0.35	5.74	3.41	0.77	0.08	0.28	0.04	29.90	0.61	245
DC4 1-2	9.14	0.36	5.07	3.02	0.69	0.05	0.40	0.02	32.01	0.61	330
DC4 2-3	10.61	0.31	6.12	3.66	0.79	0.07	0.29	0.04	29.61	0.63	245
DC4 3-4	9.37	0.38	5.68	3.00	0.66	0.05	0.34	0.05	31.37	0.68	320
DC4 4-5	10.21	0.37	6.92	3.21	0.67	0.10	0.33	0.05	29.65	0.69	270
DC4 6-7	10.60	0.32	6.32	3.61	0.77	0.11	0.30	0.05	29.47	0.66	240
DC4 8-9	11.15	0.33	5.58	3.92	0.85	0.09	0.32	0.02	29.29	0.62	---
DC4 14-15	11.26	1.44	5.70	3.93	0.95	0.11	0.32	0.05	28.27	0.61	210
DC4 19-20	10.47	7.73	6.72	3.62	1.04	0.24	0.29	0.06	24.24	0.55	165
DC4 24-25	11.53	1.44	5.85	4.10	1.26	0.10	0.34	0.04	27.59	0.61	180
DC4 29-30	11.96	0.83	6.10	4.31	1.20	0.05	0.33	0.05	27.39	0.62	150
DC4 34-35	11.72	0.99	5.93	4.16	1.14	0.04	0.30	0.08	27.73	0.63	175
DC4 39-40	11.95	0.40	6.03	4.30	1.25	0.03	0.29	0.07	27.70	0.64	155
DC4 44-45	11.74	0.62	5.66	4.29	1.20	0.05	0.32	0.04	28.04	0.63	180
DC4 49-50	10.65	0.85	5.73	3.80	1.22	0.06	0.29	0.04	29.08	0.63	215
DC4 54-55	11.02	0.97	5.75	3.99	1.20	0.06	0.29	0.04	28.59	0.62	190
Parent[a]	11.5	1.11	5.91	4.09	1.19	0.07	0.31	0.05	27.9	0.63	187

[a]parent concentrations were taken as the average of the deepest seven samples from DC4.

Table 9: DC2 Tau values, with Zr as an immobile element ($\tau_{Zr,j}$)

Sample ID	Al,$\tau_{Ti,j}$	Ca,$\tau_{Ti,j}$	Fe,$\tau_{Ti,j}$	K,$\tau_{Ti,j}$	Mg,$\tau_{Ti,j}$	Mn,$\tau_{Ti,j}$	Na,$\tau_{Ti,j}$	P,$\tau_{Ti,j}$	Si,$\tau_{Ti,j}$
DC2 6-7	-0.07	-0.78	-0.07	-0.07	-0.31	-0.21	-0.23	-0.02	-0.07
DC2 7-8	-0.19	-0.81	-0.19	-0.22	-0.36	0.20	-0.09	-0.52	-0.16
DC2 8-8.5	0.03	-0.75	-0.01	0.01	-0.17	0.09	0.03	0.05	-0.01
DC2 9-9.5	-0.20	-0.53	-0.22	-0.22	-0.34	-0.07	-0.14	-0.18	-0.13
DC2 11-13	-0.19	1.32	-0.27	-0.21	-0.34	0.29	0.00	-0.23	-0.15
DC2 13-14	-0.15	3.09	-0.04	-0.18	-0.20	0.91	-0.06	-0.06	-0.11
DC2 14-15	0.04	1.08	0.10	0.03	-0.07	0.18	0.01	-0.17	0.01
DC2 17-18	-0.03	0.10	-0.03	-0.04	-0.10	0.56	0.02	-0.05	-0.05
DC2 22-23	-0.39	4.17	-0.26	-0.41	-0.14	1.20	-0.27	-0.05	-0.28
DC2 24-25	-0.21	0.38	-0.09	-0.23	-0.11	0.43	-0.20	-0.35	-0.18
DC2 26-27	-0.06	0.55	0.02	-0.09	0.00	0.18	-0.02	-0.25	-0.10
DC2 31-32	0.13	-0.23	0.12	0.12	0.11	-0.06	0.17	0.06	0.09
DC2 36-37	0.14	-0.06	0.07	0.17	0.11	0.08	0.23	-0.04	0.09
DC2 41-42	-0.03	-0.20	-0.02	-0.04	-0.07	-0.28	-0.01	-0.24	0.00
DC2 46-47	0.05	-0.56	0.03	0.06	0.02	-0.49	0.10	0.00	0.05
DC2 51-52	-0.27	-0.15	-0.21	-0.30	-0.24	-0.21	-0.28	-0.14	-0.14
Parent[a], $C_{i,p}$	11.48	1.11	5.91	4.09	1.19	0.07	0.31	0.05	27.9

[a] Parent values were determined as an average of the 7 deepest samples from the drill cores DC2, DC3, and DC4

Table 10: DC4 Tau values, with Zr as an immobile element ($\tau_{Zr,j}$)

Sample ID	Al,$\tau_{Ti,j}$	Ca,$\tau_{Ti,j}$	Fe,$\tau_{Ti,j}$	K,$\tau_{Ti,j}$	Mg,$\tau_{Ti,j}$	Mn,$\tau_{Ti,j}$	Na,$\tau_{Ti,j}$	P,$\tau_{Ti,j}$	Si,$\tau_{Ti,j}$
DC4 0-1	-0.29	-0.76	-0.26	-0.36	-0.50	-0.06	-0.31	-0.40	-0.18
DC4 1-2	-0.55	-0.81	-0.51	-0.58	-0.67	-0.58	-0.27	-0.78	-0.35
DC4 2-3	-0.29	-0.79	-0.21	-0.32	-0.49	-0.16	-0.28	-0.34	-0.19
DC4 3-4	-0.52	-0.80	-0.44	-0.57	-0.68	-0.57	-0.36	-0.37	-0.34
DC4 4-5	-0.38	-0.77	-0.19	-0.46	-0.61	0.02	-0.28	-0.19	-0.26
DC4 6-7	-0.28	-0.77	-0.17	-0.31	-0.50	0.25	-0.26	-0.24	-0.18
DC4 14-15	-0.13	0.15	-0.14	-0.15	-0.29	0.44	-0.08	-0.04	-0.10
DC4 19-20	0.03	6.89	0.29	0.00	-0.01	3.05	0.06	0.54	-0.02
DC4 24-25	0.04	0.35	0.03	0.04	0.10	0.54	0.12	-0.19	0.03
DC4 29-30	0.30	-0.06	0.29	0.31	0.26	-0.08	0.31	0.22	0.22
DC4 34-35	0.09	-0.05	0.07	0.09	0.02	-0.34	0.01	0.88	0.06
DC4 39-40	0.26	-0.56	0.23	0.27	0.27	-0.41	0.11	0.75	0.20
DC4 44-45	0.06	-0.42	-0.01	0.09	0.05	-0.24	0.05	-0.20	0.04
DC4 49-50	-0.19	-0.33	-0.16	-0.19	-0.11	-0.24	-0.19	-0.32	-0.09
DC4 54-55	-0.06	-0.14	-0.04	-0.04	-0.01	-0.15	-0.09	-0.23	0.01
Parent[a], $C_{i,p}$	11.48	1.11	5.91	4.09	1.19	0.07	0.31	0.05	27.9

[a] Parent values were determined as an average of the 7 deepest samples from the drill cores DC2, DC3, and DC4